ISSN 1063-7834, Physics of the Solid State, 2020, Vol. 62, No. 7, pp. 1271–1279. © Pleiades Publishing, Ltd., 2020.
Russian Text © The Author(s), 2020, published in Fizika Tverdogo Tela, 2020, Vol. 62, No. 7, pp. 1123–1131.

THERMAL PROPERTIES

Thermodynamic Properties of Vanadium Oxypentafluoride (IV) $(NH_4)_3VOF_5$

E. V. Bogdanov[a, b, *], E. I. Pogoreltsev[a, c], A. V. Kartashev[a], M. V. Gorev[a, c], M. S. Molokeev[a, c], S. V. Mel'nikova[a], I. N. Flerov[a, c], and N. M. Laptash[d]

[a] *Kirensky Institute of Physics, Krasnoyarsk Scientific Center, Siberian Branch, Russian Academy of Sciences, Krasnoyarsk, 660036 Russia*

[b] *Krasnoyarsk State Agrarian University, Institute of Engineering Systems and Power, Krasnoyarsk, 660049 Russia*

[c] *Siberian Federal University, Institute of Engineering Physics and Radio Electronics, Krasnoyarsk, 660041 Russia*

[d] *Institute of Chemistry, Far Eastern Branch, Russian Academy of Sciences, Vladivostok, 690022 Russia*

**e-mail: evbogdanov@iph.krasn.ru*

Received January 22, 2020; revised January 30, 2020; accepted January 30, 2020

Abstract—The $(NH_4)_3VOF_5$ crystals have been synthesized and their homogeneity and single-phase structure has been established by the X-ray diffraction, energy dispersive spectroscopy, and X-ray photoelectron spectroscopy studies. The investigations of the temperature dependences of specific heat, entropy, strain, and pressure susceptibility show the occurrence of three phase transitions caused by the structural transformations in the $(NH_4)_3VOF_5$ crystals. The *T*–*p* phase diagram shows the temperature limits of stability of the crystalline phases implemented in $(NH_4)_3VOF_5$. The optical and dielectric studies disclose the ferroelastic nature of the phase transitions. An analysis of the experimental data together with the data on the isostructural $(NH_4)_3VO_2F_4$ crystal makes it possible to distinguish the physical properties of oxyfluorides containing vanadium of different valences (IV and V).

Keywords: oxyfluorides, phase transitions, specific heat, birefringence, thermal expansion, pressure susceptibility

DOI: 10.1134/S1063783420070057

1. INTRODUCTION

The structure of vanadium-based complex fluorides and oxyfluorides $A_2A'VO_xF_{6-x}$ (A and A' are NH_4, Cs, Rb, K, Na; $x = 0, 1, 2$) can be formed by anionic polyhedra with different symmetries due to the ability of the central atom to stably exist in different valence states [1]. In contrast to fluorides, in which the six-coordinated polyhedron $[VF_6]^{3-}$ is a regular octahedron [2], in the compounds with $x = 1$ and 2, its local symmetry is tetragonal and rhombic, respectively, which leads to the occurrence of a local polar moment [3, 4]. However, despite the latter circumstance, the crystal structure of most $A_2A'VO_2F_4$ and $A_2A'VOF_5$ compounds is highly symmetric (sp. gr. $Fm\bar{3}m$, $Z = 4$), which is caused by, at least, the disordering of fluorine-oxygen ligands [5, 6].

In ammonium oxyfluorides $(NH_4)_3VOF_5$ and $(NH_4)_3VO_2F_4$, ligands are equally distributed over two crystallographic sites 24*e* + 96*j*; however, the anionic polyhedra $[VO_2F_4]^{3-}$ and $[VOF_5]^{3-}$ have different numbers of spatial orientations (twelve and six, respectively [6]). The vibrational spectroscopy data point out the dynamic character of orientational disordering of anionic groups, which is especially pronounced in $(NH_4)_3VOF_5$ [7]. The ammonium groups are also disordered. The tetrahedron in the 4*b* site has eight spatial orientations due to the disordering of hydrogen atoms over the 96*j* sites and two tetrahedra in the 8*c* site are disordered in the 32*f* sites and characterized by four spatial orientations.

According to the data of the optical, thermal, and dielectric studies, the $(NH_4)_3VO_2F_4$ crystal undergoes a sequence of four phase transitions at temperatures of $T_1 = 438$ K, $T_2 = 244$ K, $T_3 = 210$ K, and $T_4 = 205$ K, which are accompanied by the symmetry changes $Fm\bar{3}m \leftrightarrow Immm(I222) \leftrightarrow$ rhombic $\leftrightarrow P112/m \leftrightarrow P\bar{1}$ [8, 9]. The calorimetric measurements made it possible to determine the energy characteristics of the transitions, which allow one to analyze the mechanisms of structural distortions. The total entropy change for the sequence of phase transitions in the $(NH_4)_3VO_2F_4$ crystal ($\sum_i \Delta S_i \approx 17$ J/mol K) appeared to be much smaller than the entropy that follows from the model of disordering of structural elements in the $Fm\bar{3}m$

phase ($\sum_i \Delta S_i \approx 34$ J/mol K) [6]. An essential role of the ammonium cation in the structural distortions was established in studying the deuterated $(ND_4)_3VO_2F_4$ crystal [10]. The deuteration changed the chemical pressure and, consequently, the temperature of the phase transitions and reduced the anharmonicity of the vibrations of tetrahedral cations, which led to a decrease in the total entropy ($\sum_i \Delta S_i \approx 15$ J/mol K) as compared with the protonated $(NH_4)_3VO_2F_4$ crystal [9].

According to the results of prospective studies, the $(NH_4)_3VOF_5$ crystals undergo a sequence of three phase transformations $Fm\bar{3}m \leftrightarrow Immm \leftrightarrow ? \leftrightarrow ?$ at temperatures of $T_1 = 349$ K, $T_2 = 230$ K, and $T_3 = 221$ K [6]. Despite the detailed study of the structure of the $Fm\bar{3}m$ and $Immm$ phases, data on their physical properties are lacking, which complicates the analysis of the nature and mechanism of the phase transitions.

In this work, we investigate the optical, thermal, structural, and dielectric properties of the $(NH_4)_3VOF_5$ crystal in wide temperature and pressure ranges. The effect of external hydrostatic and chemical pressures on the stability of the implemented distorted phases is established.

2. EXPERIMENTAL

The initial ammonium oxofluorovanadate crystals were synthesized by the mechanochemical interaction of the initial vanadium oxides (vanadates) with ammonium hydrodifluoride (NH_4HF_2, the melting point is $T_{melt} = 126$°C) [6]. In the course of the reaction occurring during grinding of the components under standard conditions, the initial $(NH_4)_3VO_2F_4$ and $(NH_4)_3VF_6$ complexes were obtained:

$$NH_4VO_3 + 2NH_4HF_2 = (NH_4)_3VO_2F_4 + H_2O,$$

$$VF_3 + 3NH_4HF_2 = (NH_4)_3VF_6 + 3HF.$$

Upon further dissolution of stoichiometric amounts of the obtained complexes in water upon heating in a water bath and subsequent slow evaporation of the greenish-blue solution, well-faceted bright blue $(NH_4)_3VOF_5$ octahedra crystallized:

$$(NH_4)_3VO_2F_4 + (NH_4)_3VF_6 = 2 \cdot (NH_4)_3VOF_5.$$

The energy dispersive X-ray spectroscopy analysis on a Hitachi 5500 high-resolution electron scanning microscope with an EDS Thermo Scientific energy dispersive attachment confirmed the $(NH_4)_3VOF_5$ composition of the single crystals with an O : F ratio close to 1 : 5.

The synthesized crystals were investigated by X-ray photoelectron spectroscopy. The X-ray photo-emission spectra provided information on the nature of chemical bonds of the investigated elements. The

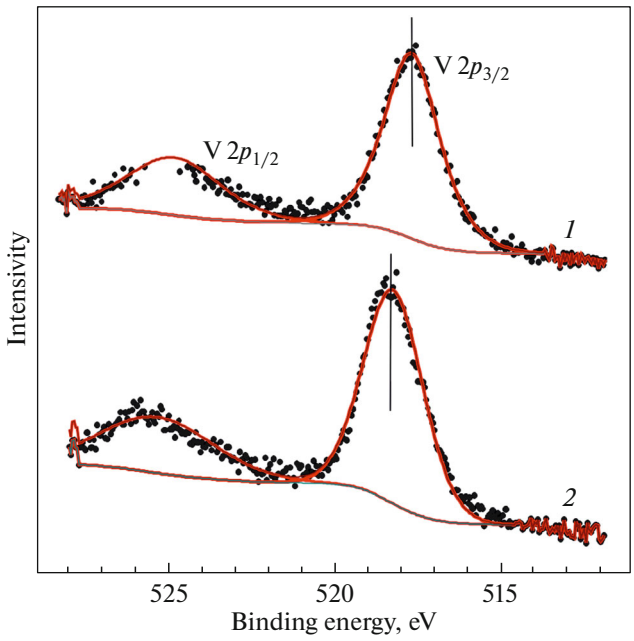

Fig. 1. X-ray photoemission spectra for (*1*) $(NH_4)_3VOF_5$ and (*2*) $(NH_4)_3VO_2F_4$.

binding energies calculated from the spectra (the $V2p_{3/2}$ line) for the initial $(NH_4)_3VO_2F_4$ and investigated $(NH_4)_3VOF_5$ crystals were found to be $E_b = 518.3$ eV and $E_b = 517.7$ eV, respectively (Fig. 1). A significant difference of $\Delta E_b = 0.6$ eV between the binding energies makes it possible to unambiguously identify the vanadium compounds. In addition, the spectra show that the grown $(NH_4)_3VOF_5$ crystals contain vanadium in the only form V^{4+}.

The data on the $(NH_4)_3VO_2F_4$ structure were obtained by X-ray diffraction using a Bruker D8 ADVANCE powder diffractometer (K_αCu radiation) and a VANTEC linear detector ($2\theta \approx 0.016°$, $t \approx 0.2s/2\theta$). The investigations were carried out in the temperature range of 133–423 K with a step of ~10 K using an Anton Paar TTK450 temperature chamber.

The model of the high-temperature phase structure was refined by the Rietveld method (Fig. 2) using the TOPAS 4.2 program [11]. The indexing of the X-ray diffraction patterns obtained in the temperature range of 353–423 K showed that the unit cell is cubic face-centered (sp. gr. $Fm\bar{3}m$, $Z = 4$, see Table 1); no additional reflections were observed.

With a decrease in temperature, the main reflections of the cubic phase are split (Fig. 3), which, according to the homology method [12], indicates the occurrence of a rhombic structure at room temperature. Below the phase transition temperature $T_1 = 349$ K, superstructural reflections are observed, which correspond to the instability at the point $k = (2/3, 2/3, 0)$ of the Brillouin zone, indicating a significant (by a

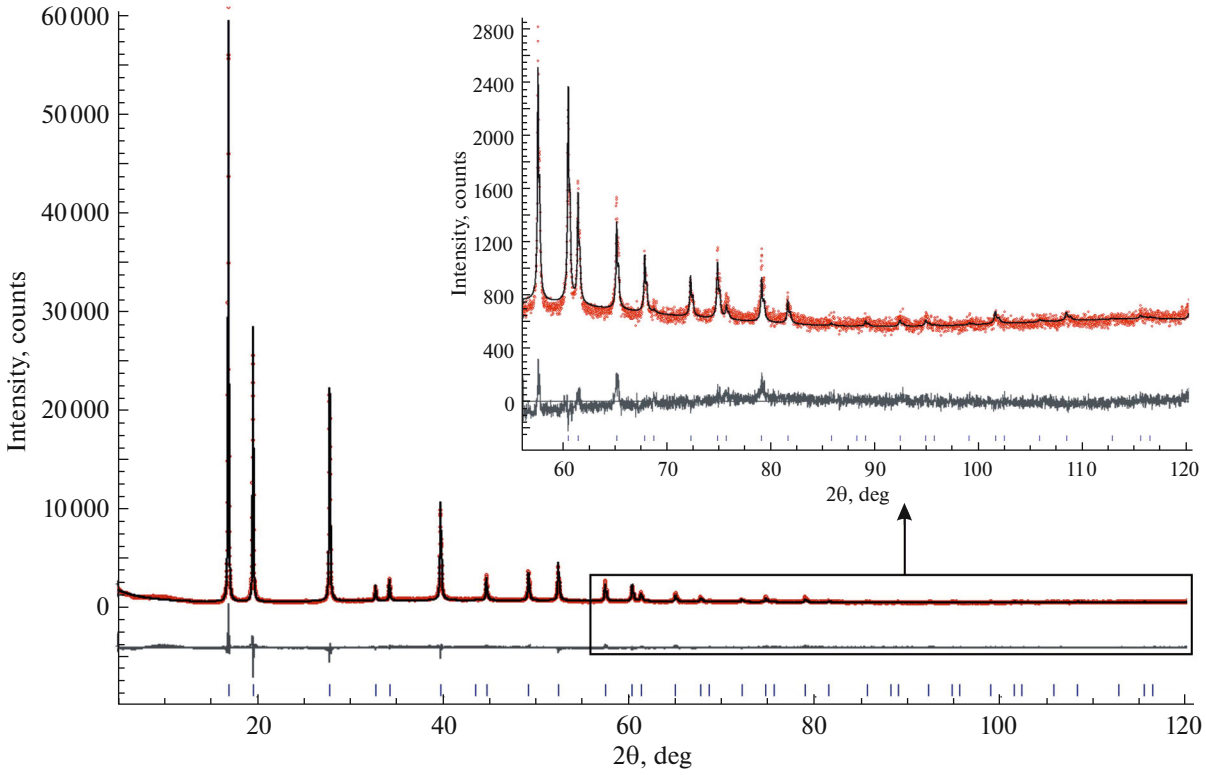

Fig. 2. Rietveld difference X-ray diffraction pattern obtained by refining of the $(NH_4)_3VOF_5$ crystal structure in the cubic phase ($T = 383$ K).

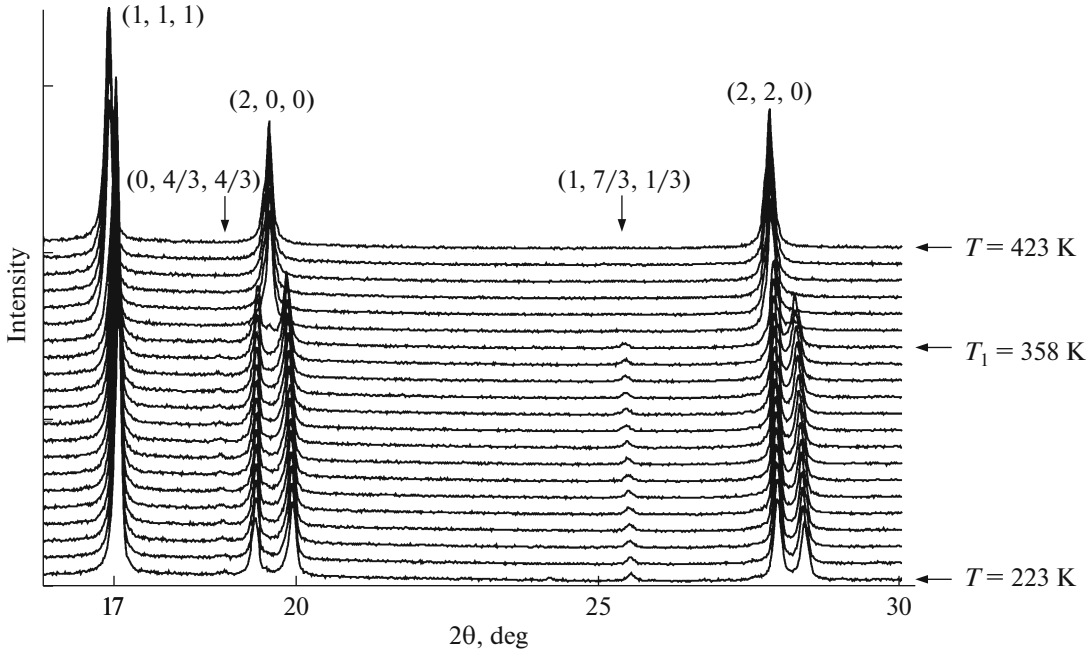

Fig. 3. Fragment of the $(NH_4)_3VOF_5$ X-ray diffraction patterns at temperature T ranging within 223—423 K with a step of $\Delta T = 10$ K. Cubic cell indices are given in parenthesis.

Table 1. Main parameters of the refinement of the $(NH_4)_3VOF_5$ crystal structure (sp. gr. $Fm\bar{3}m$): a and V are the unit cell parameter and volume; Z is the number of formula units in the cell, M_r is the relative molecular weight of the formula unit; 2θ is the angular range of the X-ray diffraction pattern; R_p, R_{wp}, R_B are the profile, weight profile, and Bragg reliability factors, respectively; and χ^2 is the R_{wp}/R_{exp} fitting quality, where R_{exp} is the expected profile factor

Parameter	Value
a, Å	9.0710(2)
V, Å^3	746.38(4)
Z	4
M_r	216.05
2θ	5–120
R_{wp}, %	7.677
R_p, %	6.089
R_{exp}, %	3.292
χ^2	1.11
R_B, %	2.87

factor of at least 3) increase in the unit cell volume. The indexing and refinement of the X-ray profile showed that the unit cell is described by the space group $Immm$: $a = 9.1685(2)$ Å, $b = 18.9112(8)$ Å, and $c = 6.3014(3)$ Å. The parameters of the rhombic cell significantly change as compared with the parameters of the cubic cell: $a_{orth} = a_{cub}$, $b_{orth} = 3b_{cub}/2 + 3c_{cub}/2$, $c_{orth} = b_{cub}/2 - c_{cub}/2$, where a_{orth}, b_{orth}, and c_{orth} are the basis vectors of the rhombic cell and a_{cub}, b_{cub}, and c_{cub} are the basis vectors of the cubic cell (Fig. 4).

With a further decrease in temperature, the main reflections are slightly split, which can be related to the occurrence of one more or even several phase transitions. In this case, the crystal cell becomes either monoclinic or triclinic. An analysis of the superstructural reflections showed that they correspond to the occurrence of instability at the points $k = (1/2, 1/2, 1/2)$ and $k = (1/2, 0, 0)$ of the Brillouin zone. Then, the minimum unit cell volume becomes larger than the cubic unit cell volume by a factor of 12 and it is difficult to establish the cell parameters of such a distorted phase.

The optical investigations were carried out using an Axioskop-40 polarizing microscope and a Linkam LTS 350 temperature camera. The temperature study was carried out in a quasi-static mode with an accuracy of ±0.1 K in the temperature range of 100–400 K. The extinction position and indicatrixe rotation angle were determined accurate to ~0.5°. Birefringence was measured with a Berek (Leica) compensator accurate to ~0.00001.

Thin (30–100 μm) $(NH_4)_3VOF_5$ growth plates oriented in the (111) and (110) planes of the cubic crystal structure were selected for investigations. In the high-temperature region, the $(NH_4)_3VOF_5$ sample is optically isotropic, $\Delta n = 0$ (Figs. 5a and 5b), which confirms the initial cubic symmetry of the crystal.

Below 350 K, a twinned picture appears in the microscope field of view (Fig. 5c), which has a form of wide bands with boundaries tilted at an angle of 120°, indicating that the crystal loses its third-order axis upon cooling at temperature $T_{1\downarrow}$. The direct extinction of the formed twins along the [110] direction also confirms the rhombic symmetry implementation at room temperature.

The phase transition is accompanied by a stepwise occurrence of the optical anisotropy (Fig. 5a). Upon heating, the phase transition temperature $T_{1\uparrow}$ depends on the heating rate and can change between 349–357 K, while upon cooling, the temperature $T_{1\downarrow}$ is almost constant and amounts to 338 K. The measurements of $\Delta n(T)$ in the quasi-static mode with a step of $\Delta T \approx 0.1$ K made it possible to determine equilibrium phase transition temperatures of $T_{1\uparrow} = 357.1$ K and $T_{1\downarrow} = 338.1$ K. The significant hysteresis $\delta T_1 \approx 19$ K unambiguously shows that the high-temperature phase transition is a first-order transformation.

Upon cooling below 230 K, the twin picture becomes much more complicated and the extinction of the sample completely vanishes (Fig. 5d). Upon first cooling, the $\Delta n(T)$ anomaly is observed at a temperature of $T_{3\downarrow} \approx 218$ K, which is accompanied by the occurrence of additional twinning of the crystal. Upon heating, $\Delta n(T)$ occurs at a higher temperature of $T_{2\uparrow} = 228$ K and this value is reproduced upon further heating/cooling of the sample.

The absence of extinction in the samples at low temperatures is indicative of the lowest crystal symmetry group $P\bar{1}$ or $P1$ in this phase and the anomalous stepwise behavior of birefringence (Fig. 5a) speaks about the presence of some intermediate (monoclinic) phase.

To obtain information on the amount, temperature, and integrated energy characteristics of the phase transitions in the $(NH_4)_3VOF_5$ crystals, the temperature dependence of specific heat $C_p(T)$ was studied by adiabatic calorimetry. The investigated sample with a total mass of ~1.1g was hermetically sealed in a furniture with a heater in the inert helium atmosphere. The specific heat of the system was measured in the continuous ($dT/dt = 0.15$ K/min) and discrete ($\Delta T = 2.5$–3.0 K) heating modes. The specific heat of the furniture was measured in a separate experiment.

The temperature dependence of the molar isobaric specific heat $C_p(T)$ of the $(NH_4)_3VOF_5$ crystals exhibits the anomalous behavior at refined phase transitions temperatures of $T_1 = 348.1 \pm 0.5$ K, $T_2 = 229.1 \pm$

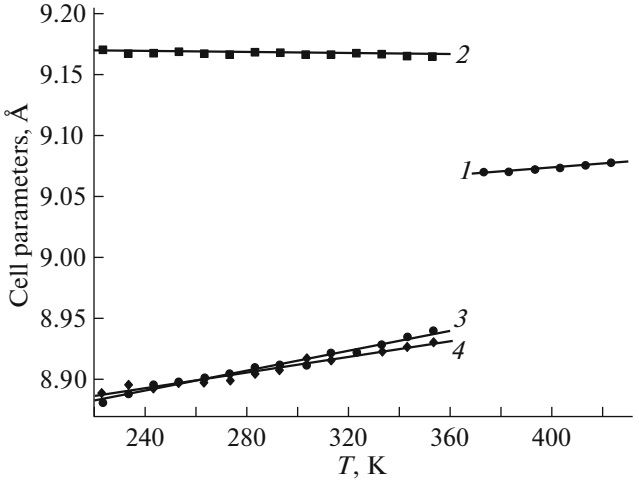

Fig. 4. Temperature dependences of the $(NH_4)_3VOF_5$ cell parameters: (*1*) a_{cub}, (*2*) a_{orth}, (*3*) $b_{orth}\sqrt{2}/3$, and (*4*) $c_{orth}\sqrt{2}$.

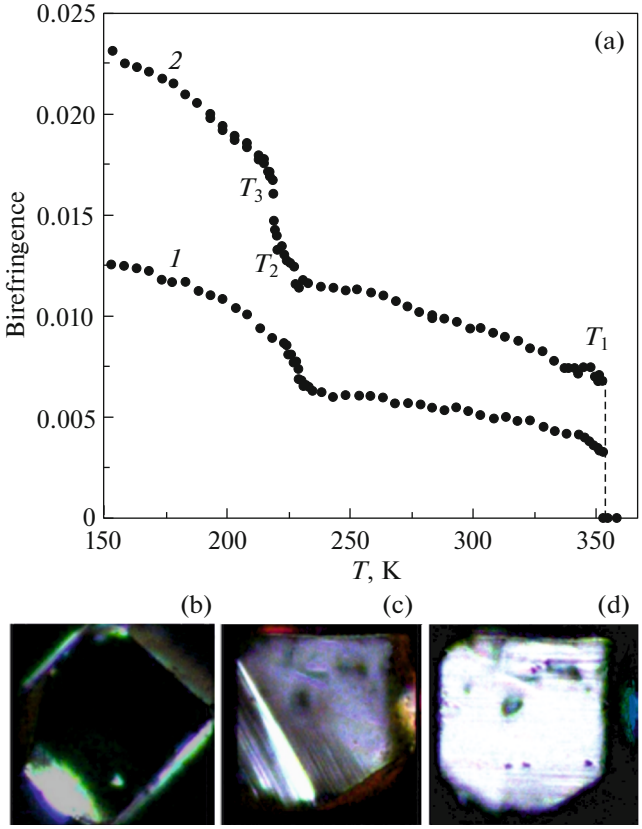

Fig. 5. (a) Temperature dependences of birefringence in (*1*) the (111) and (*2*) (110) cubic phases of the $(NH_4)_3VOF_5$ crystal. Polarization optics observation of the (111) cubic-phase samples in (b) the $Fm\bar{3}m$, (c) *Immm*, and (d) $P\bar{1}$ phases.

0.2 K, and $T_3 = 218 \pm 1$ K (Fig. 6a). To determine the integral characteristics, the specific heat was divided into the regular contribution and the anomalous contribution $\Delta C_p(T)$ related to the sequence of transitions. To do that, portions in the temperature dependence of the specific heat beyond the region of existence of the anomalies were approximated by a combination of the Debye and Einstein functions. Integrating the temperature dependence of the excess specific heat $\Delta C_p(T)$, we obtained the entropy changes $\Delta S_i = \int (\Delta C_p/T)dT$, which characterize the phase transformations in $(NH_4)_3VOF_5$: $\Delta S_i = 5.4 \pm 0.5$ J/mol K and $\Delta S_{2+3} = 8 \pm 0.5$ J/mol K (Fig. 6b).

The thermal expansion was measured on a NETZSCH DIL 402C dilatometer in the temperature range of 120–350 K in the dynamic mode at a heating rate of 3 K/min. The investigations were carried out in a gaseous helium stream at a flow rate of 50 mL min^{-1}. To calibrate the device and take into account the thermal expansion of the measuring system, fused silica standards were used [13]. The $(NH_4)_3VOF_5$ samples were pressed in tablets with a diameter of ~4 mm and a height of ~4–6 mm at a pressure of ~2 GPa.

In the temperature range of the phase transitions, the thermal expansion exhibited the anomalous behavior (Fig. 7). A significant strain jump of $\delta(V/V_0) = 1 \times 10^{-4}$ K characterizes the transition at temperature T_1 as a first-order transformation. In the low temperature region, the anomalies of the volumetric thermal expansion coefficient are more pronounced: $\Delta\beta(T_2) = 0.62 \times 10^{-4}$ K^{-1} and $\Delta\beta(T_3) = 0.24 \times 10^{-4}$ K^{-1}.

The susceptibility to the hydrostatic pressure was studied using differential thermal analysis (DTA). A polycrystalline sample with a mass of ~0.02 g was packed in a copper container attached to one of the junctions of a thermoelectric DTA element. The measurements were performed in a high-pressure cylinder–piston chamber; silicone oil was used as a medium for transmitting the hydrostatic pressure.

The pressure susceptibility of the high-temperature phase transition cannot be directly measured because of the temperature limitations imposed on the DTA setup.

The phase transition temperatures T_2 and T_3 increase almost linearly with the external pressure (Fig. 8). Due to the significant difference between the pressure coefficients $dT_2/dp = 23 \pm 2$ K/GPa and $dT_3/dp = 92 \pm 4$ K/GPa, a triple point is observed in the T–p phase diagram at a pressure of $p \approx 0.1$ GPa. The susceptibility of the phase boundary *Immm* $\leftrightarrow$ $P\bar{1}$ ($P1$) formed at high pressure is characterized by a sufficiently large baric coefficient $dT^*/dp = 80 \pm 1$ K/GPa.

The temperature dependence of the permittivity was examined with an E7-20 immitance meter at a frequency of 1 kHz in the temperature range of 100–320 K. The $(NH_4)_3VOF_5$ samples were prepared in the

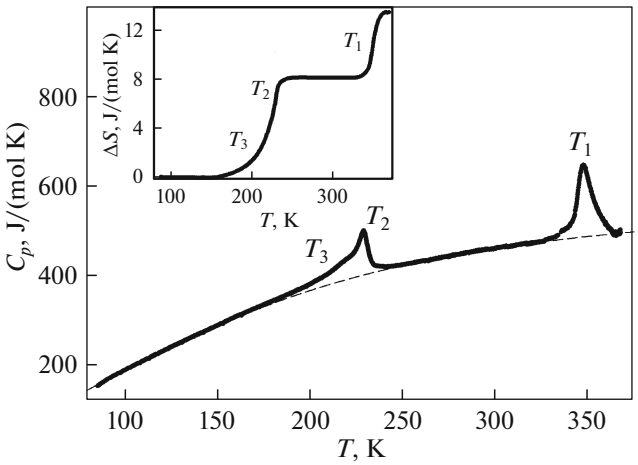

Fig. 6. Temperature dependences of the specific heat and entropy of the phase transitions (inset) in the $(NH_4)_3VOF_5$ crystal in a wide temperature range.

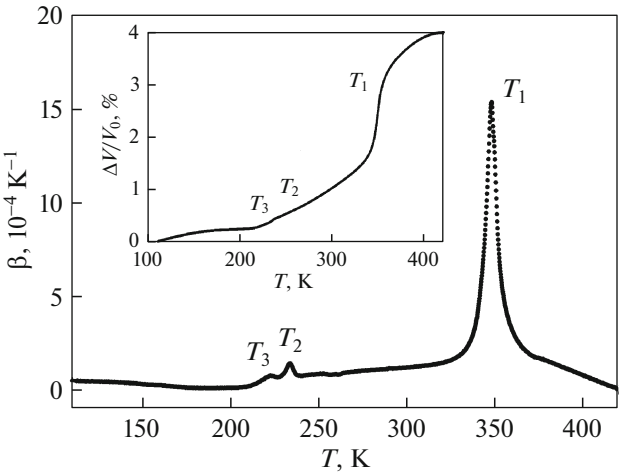

Fig. 7. Temperature dependences of the volume expansion coefficient and strain coefficient (inset) of the $(NH_4)_3VOF_5$ crystal.

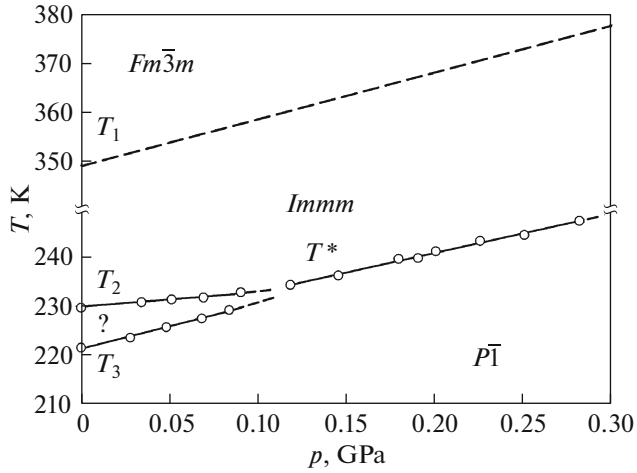

Fig. 8. Temperature–pressure phase diagram of the $(NH_4)_3VOF_5$ crystal. The interface between the $Fm\bar{3}m$ and *Immm* phases (dashed line) is reconstructed using the calculation of $(dT_1/dp)_{calc}$.

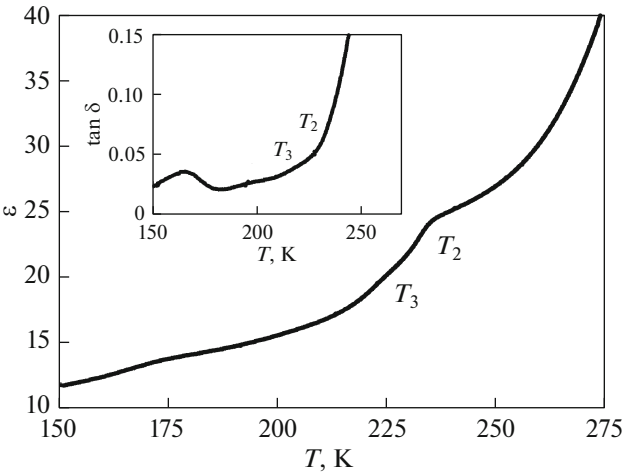

Fig. 9. Temperature dependences of the permittivity ε(T) and dissipation factor tanδ(T) (inset) for the $(NH_4)_3VOF_5$ crystals.

form of tablets with a diameter of ~8 mm and a height of ~1–2 mm at a pressure of ~2 GPa. Electrodes were formed by vacuum deposition of gold onto the samples. The temperature variation rate in the heating and cooling modes was ~0.7 K/min.

In the temperature dependences of the permittivity ε(T) and dissipation factor tanδ(T) (Fig. 9) in the region of phase transitions at temperatures T_2 and T_3, a stepwise increase in the permittivity $\Delta\varepsilon_1 \approx \Delta\varepsilon_2 \approx 2$ is observed. This ε(T) behavior is characteristic of nonferroelectric phase transitions. The anomalous behavior in the region of the high-temperature phase transition is accompanied by a significant increase in the permittivity, which is caused by the noticeable growth of the dissipation factor in the high-temperature region of $T > 270$ K (Fig. 9b).

3. RESULTS AND DISCUSSION

The paraphase of the investigated $(NH_4)_3VOF_5$ compound is isostructural to elpasolite (sp. gr. $Fm\bar{3}m$, $Z = 4$) [14, 15]. Based on the analysis of the structural data, F and O atoms occupy the same 24*e* site with populations of 5/6 and 1/6 (Table 2). Their combined thermal parameter was refined in the anisotropic approximation. However, additional maxima in the 48*h* site corresponding to F(O), O1(F1), and O2(F2) atoms were found in the electron density. Therefore, in

Table 2. Atomic coordinates, position populations p, and isotropic (B_{iso}) and anisotropic (U_{ij}) thermal parameters of the $(NH_4)_3VOF_5$ at $T = 383$ K

Atom	x	y	z	p	B_{iso}/U_{ij}
V	0	0	0	1	5.8(2)
N1	1/2	1/2	1/2	1	12.4(4)
H1	0.55	0.55	0.55	0.5	
N2	1/4	1/4	1/4	1	7.1(3)
H2	0.198	0.198	0.198	1	5
F1	0.2098(4)	0	0	0.691(8)	$U_{11} = 0.011(5)$ $U_{22} = U_{33} = 0.173(5)$
O1	0.2098(4)	0	0	0.138(2)	$U_{11} = 0.011(5)$ $U_{22} = U_{33} = 0.173(5)$
F2	0.366(2)	0.366(2)	0	0.071(4)	5.0(8)
O2	0.366(2)	0.366(2)	0	0.0143(8)	5.0(8)

the final refinement, two sites, O1/F1 and O2/F2, were used. The populations of the sites were limited by linear equations so that the resulting formula was $(NH_4)_3VOF_5$.

As a result of the phase transition, the $(NH_4)_3VOF_5$ structure changes for rhombic (sp. gr. *Immm*) and has the cell parameters similar to those of the $(NH_4)_3VO_2F_4$ crystal [6]. Owing to the strong twinning, the $(NH_4)_3VO_2F_4$ crystal structure was not completely determined even for a single crystal [6, 8]; therefore, the model of disordering of one of the two independent $[VO_2F_4]^{3-}$ polyhedra was not reliably established. The model of disorder of $(NH_4)_3VOF_5$ cannot be established from the X-ray data either.

The temperature dependence of the unit cell volume contains a noticeable volume jump of $\Delta V_c \approx 13.8$ Å, which is observed at the phase transformation at T_1 (Fig. 10). Thus, the high-temperature transformation is a first-order phase transition. The information on the change ΔS_1 in the entropy of the high-temperature phase transition obtained from the conducted thermal experiments allows us to estimate the slope of the phase boundary $Fm\bar{3}m \leftrightarrow Immm$. The pressure coefficient was determined from the Clausius–Clapeyron equation $dT/dp_1 = (\Delta V N_A)/(Z\Delta S) \approx 128$ K/GPa, where ΔV is the change in the cubic cell volume during the phase transition, N_A is the Avogadro number, and $Z = 4$ is the number of formula units in the cell.

The study of the $C_p(T)$ dependence revealed the presence of the excess specific heat in a fairly wide temperature range below T_2 (Fig. 11a), which allowed us to analyze the phase transformation *Immm* ↔ monoclinic phase in the framework of the Landau thermodynamic theory. According to [16], the squared inverse excess specific heat is a linear function of temperature: $(\Delta C_p/T)^{-2} = [2(B^2 - 3A'C)^{0.5}/A_T^2]^2 + 12C(T_0 - T)/A_T^3$, where the quantities $A = A_T(T_0 - T_C) + A_T(T - T_0) = A' + A_T(T - T_0)$, B, and C are the coefficients of the thermodynamic potential $\Delta\Phi(p, T, \eta) = A\eta^2 + B\eta^4 + C\eta^6$ (η is the transition parameter, T_C is the Curie temperature, and T_0 is the phase transition temperature). The temperature behavior of the squared inverse excess specific heat of $(NH_4)_3VOF_5$ below temperature T_2 is described fairly well by a linear function (Fig. 11b). The calculated parameters of the phenomenological model of the phase transition at T_2 (Table 3) show that, in the $(NH_4)_3VOF_5$ crystals, the transformation *Immm* ↔ monoclinic phase is located farther from the tricritical point ($T_i - T_{Ci} = 0$ and $N = 0$, where $N = \pm[B^2/(3A_TCT_0)]^{-0.5}$ is the degree of proximity of the transition to the tricritical point) than the phase transition *Immm* ↔ $P112/m$ observed in

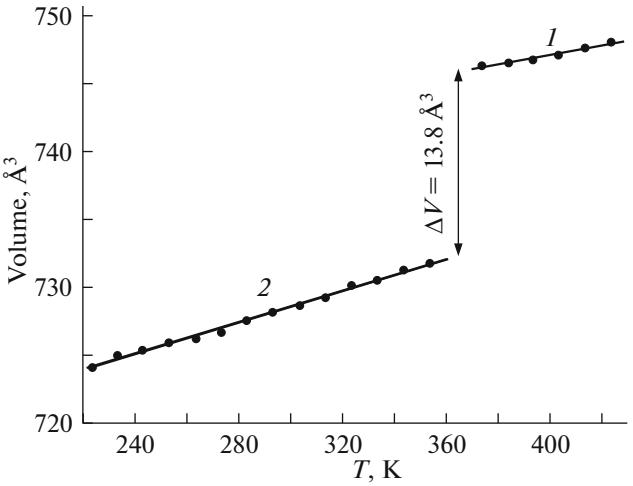

Fig. 10. Temperature dependences of the cell volume (*1*) V_{cub} and (*2*) $V_{orth}2/3$.

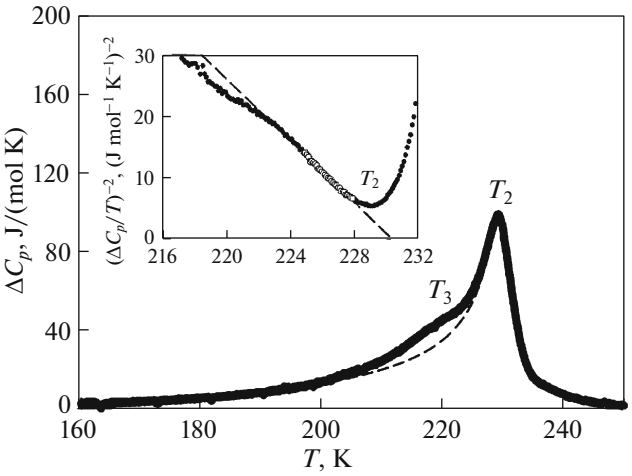

Fig. 11. Temperature dependences of the excess specific heat and its reciprocal quantity (inset) in the vicinity of T_2.

$(NH_4)_3VO_2F_4$ at temperature T_3 [9]. The extrapolation of the $(\Delta C_p/T)^{-2}(T)$ dependence obtained using the phenomenological model allows us to separate the energy contributions of the phase transitions at temperatures T_2 and T_3 (Fig. 11a) and estimate the value of individual entropy changes ΔS_2 and ΔS_3 (Table 3).

Table 3. Thermodynamic parameters of the phase transitions in the $(NH_4)_3VOF_5$ and $(NH_4)_3VO_2F_4$ oxyfluorides

Parameter	$(NH_4)_3VOF_5$	$(NH_4)_3VO_2F_4$ [9]
T_1, K	348.1 ± 0.5	438 ± 1
ΔS_1, J/mol K	5.4 ± 0.5	9.7 ± 1.0
$(dT_1/dp)_{calc}$, K GPa^{-1}	115 ± 10	–
T', K		244.0 ± 0.2
$\Delta S'$, J/mol K		0.18 ± 0.04
T_2, K	229.1 ± 0.2	210.2 ± 0.2
$(A_T^2/B)_{T_2}$, J/mol K^2	–0.6	–0.4
$(A_T^3/C)_{T_2}$, J^2/mol^2 K^3	4.6	1.1
$T_2 - T_{C_2}$, K	3.2	1.4
N_2	–0.13	–0.1
ΔS_2, J/mol K	7.6	6.2 ± 0.7
$(dT_2/dp)_{exp}$, K GPa^{-1}	23 ± 2	–27 ± 3
T_3, K	218 ± 1	205.1 ± 0.2
$(A_T^2/B)_{T_3}$, J/mol K^2	–	–1.3
$(A_T^3/C)_{T_3}$, J^2/mol^2 K^3	–	2.2
$T_3 - T_{C_3}$, K	–	0.4
N_3	–	–0.05
ΔS_3, J/mol K	0.4 ± 0.06	0.80 ± 0.12
$(dT_3/dp)_{exp}$, K GPa^{-1}	92 ± 4	–25 ± 3

A joint analysis of the experimental data on the specific heat and thermal expansion made it possible to calculate the pressure susceptibility of the crystal phases implemented in $(NH_4)_3VOF_5$. Using the entropy jumps $\Delta S_1 \approx 2.8$ J/mol K (Fig. 7b) and the strain $\delta(\Delta V/V_0) = 0.01$ (Fig. 8a) at T_1, the corresponding total pressure coefficient $(dT_1/dp)_{calc} \approx 115$ K/GPa was calculated from the Clausius–Clapeyron equation. The similar dT_1/dp values obtained from the X-ray and dilatometric data point out the reliability of the results of independent experiments.

For the low-temperature phase transitions, the pressure coefficients $(dT_2/dp)_{calc} \approx 26$ K/GPa and $(dT_3/dp)_{calc} \approx 120$ K/GPa were determined using the Ehrenfest relation $\Delta C_p = \Delta\beta T_i/(dT_i/dp)_{p=0}$ [17]. Despite the complexity of determining individual parameters of the low-temperature phase transitions, the agreement between the experimental and calculated pressure coefficients can be considered satisfactory (Table 3).

Substitution of the central atom, $V^{4+} \rightarrow V^{5+}$, led to an increase in the $(NH_4)_3VOF_5$ unit cell volume (V_c = 746 Å^3) as compared with the $(NH_4)_3VO_2F_4$ unit cell volume (V_c = 735 Å^3 [5]), which can be attributed to a decrease in the chemical pressure. Taking into account the positive sign of the pressure coefficient dT_1/dp for $(NH_4)_3VOF_5$, this should increase the temperature of stability of the cubic phase in $(NH_4)_3VO_2F_4$, which was observed in the experiments (Table 3). The estimated excess chemical pressure is $\Delta p = 0.8$ GPa.

In the structural model [6], the initial $(NH_4)_3VOF_5$ cubic phase is characterized by the disordering of both the fluorine oxygen anion $[VOF_5]^{3-}$ and ammonium cations, which should lead to the great entropy during the phase transitions. However, the experimental value of $\sum_i S_i \approx 14$ J/mol K appeared to be relatively low, although typical of the order-disorder processes. A similar situation was observed in the investigations of the isostructural $(NH_4)_3VO_2F_4$ crystal, in which even stronger disordering of structural elements was assumed [6]. However, the total entropy change related to the sequential transformations and established in the thermal investigations [9] was found to be slightly higher than the value for $(NH_4)_3VOF_5$.

4. CONCLUSIONS

The single-phase ammonium oxopentafluorovanadate (IV) $(NH_4)_3VOF_5$ crystals were synthesized. The analysis of the results of the optical, thermal, structural, and dielectric investigations together with the data obtained previously for the isostructural

$(NH_4)_3VO_2F_4$ compound [6, 9] made it possible to establish the features of the physical properties of oxyfluorides containing vanadium of different valences (IV, V).

A decrease in the chemical pressure in $(NH_4)_3VOF_5$ caused by an increase in the unit cell volume as compared with $(NH_4)_3VO_2F_4$ is accompanied by

(i) a significant change in the phase transition temperature and stability ranges of the initial and distorted phases;

(ii) a decrease in the phase transition entropies, which is qualitatively consistent with the models of the cubic structure disordering [6];

(iii) wedging out the intermediate monoclinic phase in $(NH_4)_3VOF_5$ at a relatively low pressure;

(iv) the preservation of the ferroelastic (nonferroelectric) origin of the structural distortions;

(v) a slight change in the degree of proximity of the phase transitions to the tricritical point.

ACKNOWLEDGMENTS

The authors are grateful to A.S. Romanchenko for presenting the X-ray photoelectron spectroscopy data. The X-ray and dilatometric data were obtained using the equipment of the Krasnoyarsk Territorial Center for Collective Use, Krasnoyarsk Scientific Center, Siberian Branch, Russian Academy of Sciences.

FUNDING

This study was supported by the Russian Foundation for Basic Research, the Government of the Krasnoyarsk Territory, and the Krasnoyarsk Territorial Foundation for Support of Scientific and R&D Activity, project no. 18-42-243003 "Effect of Deuteration on Orientational Ordering and Phase Transitions in Ammonium Fluorine-Oxygen Vanadates."

CONFLICT OF INTEREST

The authors declare that they have no conflicts of interest.

REFERENCES

1. G. Pausewang and K. Dehnicke, Z. Anorg. Allg. Chem. **369**, 265 (1969).
2. I. N. Flerov, M. V. Gorev, K. S. Aleksandrov, A. Tressaud, J. Grannec, and M. Couzi, Mater. Sci. Eng. **24**, 81 (1998).
3. R. Gautier, M. D. Donakowski, and K. R. Poeppelmeier, J. Solid State Chem. **195**, 132 (2012).
4. S. J. Patwe, A. S. Nagabhusan, K. G. Girija, C. G. Sivan Pillai, and A. K. Tyagi, J. Mater. Res. **25**, 1251 (2010).
5. M. Leimkühler and R. J. Mattes, Solid State Chem. **65**, 260 (1986).
6. A. A. Udovenko, E. I. Pogoreltsev, Y. V. Marchenko, and N. M. Laptash, Acta Crystallogr., B **73**, 1 (2017).
7. Yu. V. Gerasimova, A. S. Oreshonkov, N. M. Laptash, A. N. Vtyurin, A. S. Krylov, N. P. Shestakov, A. A. Ershov, and A. G. Kocharova, Spectrochim. Acta, A **176**, 106 (2017).
8. S. V. Mel'nikova and A. G. Kocharova, Phys. Solid State **51**, 597 (2009).
9. V. D. Fokina, M. V. Gorev, A. G. Kocharova, E. I. Pogoreltsev, and I. N. Flerov, Solid State Sci. **11**, 836 (2009).
10. E. V. Bogdanov, E. I. Pogoreltsev, M. V. Gorev, M. S. Molokeev, and I. N. Flerov, Phys. Solid State **61**, 192 (2019).
11. *Bruker AXS TOPAS V4: General Profile and Structure Analysis Software for Powder Diffraction Data, User's Manual* (Bruker AXS, Karlsruhe, Germany, 2008).
12. V. I. Mikheev, *X-Ray Mineral Determinant* (Geol. Okhrana Nedr, Moscow, 1957) [in Russian].
13. M. V. Gorev, E. V. Bogdanov, I. N. Flerov, A. G. Kocharova, and N. M. Laptash, Phys. Solid State **52**, 167 (2010).
14. M. S. Molokeev and S. V. Misyul', Phys. Solid State **54**, 155 (2012).
15. V. D. Fokina, I. N. Flerov, M. S. Molokeev, E. I. Pogorel'tsev, E. V. Bogdanov, A. S. Krylov, A. F. Bovina, V. N. Voronov, and N. M. Laptash, Phys. Solid State **50**, 2175 (2008).
16. K. S. Aleksandrov and I. N. Flerov, Sov. Phys. Solid State **21**, 197 (1979).
17. N. G. Personage and L. A. K. Staveley, *Disorder in Crystals* (Oxford Univ. Press, London, 1978)

Translated by E. Bondareva